

# Damping of the baryon acoustic oscillations in the matter power spectrum as a probe of the growth factor

Hidenori Nomura<sup>1</sup>, Kazuhiro Yamamoto<sup>1</sup> and Takahiro Nishimichi<sup>2</sup>

<sup>1</sup> Graduate School of Sciences, Hiroshima University, Higashi-Hiroshima, 735-8526, Japan

<sup>2</sup> Department of Physics, School of Science, The University of Tokyo, Tokyo 113-0033, Japan

E-mail: [hide@theo.phys.sci.hiroshima-u.ac.jp](mailto:hide@theo.phys.sci.hiroshima-u.ac.jp)

**Abstract.** We investigate the damping of the baryon acoustic oscillations (BAO) signature in the matter power spectrum due to the quasi-nonlinear clustering of density perturbations. On the basis of the third order perturbation theory, we construct a fitting formula of the damping in an analytic way. This demonstrates that the damping is closely related with the growth factor and the amplitude of the matter power spectrum. Then, we investigate the feasibility of constraining the growth factor through a measurement of the damping of the BAO signature. An extension of our formula including higher order corrections of density perturbations is also discussed.

## 1. Introduction

The baryon acoustic oscillations (BAO) imprinted in the galaxy power spectrum have recently attracted remarkable attention, as a useful probe for exploring the origin of dark energy [1, 2]. The BAO signature has been clearly detected in the 2dFGRS and the SDSS galaxy samples [3, 4, 5, 6, 7]. The feasibility of constraining the equation of state parameter of dark energy  $w$  is demonstrated [8, 9, 10], where  $w$  is defined by  $w = p_{de}/\rho_{de}$ , where  $p_{de}$  and  $\rho_{de}$  are the pressure and the energy density of the dark energy component, respectively. Furthermore, a lot of BAO survey projects are under progress, or planned [11, 12, 13, 14, 15, 16].

Though these BAO surveys will precisely measure the galaxy power spectra, but we also need precise theoretical templates, in order to obtain a useful cosmological constraint from observational data. In practice, we need to solve uncertainties about the gravitational nonlinear clustering of the density perturbations, the redshift-space distortions, and the galaxy clustering bias, because these uncertainties might yield some systematic effects in the BAO signature. Then, a lot of works related to these topics have been done recently, which are very important and challenging for future research of dark energy [17, 18, 19, 20, 21, 22, 23, 24, 25, 26, 27].

In the present paper, we focus on the damping of the BAO signature in the matter power spectrum due to the nonlinear gravitational clustering. We investigate this damping in a semi-analytic way on the basis of the third order perturbation theory of density fluctuations. The nonlinear clustering is a consequence of mode-couplings of the density fluctuations and the peculiar velocity divergence in Fourier space. Especially, we demonstrate how the damping of the BAO signature can be expressed with/without  $P_{22}(k)$  and  $P_{13}(k)$ , which describe the mode-coupling (see sections 2 and 3). Then, we develop a simple fitting formula relevant to the damping, which demonstrates the fact that the damping of the BAO signature is closely related with the growth factor and the amplitude of the matter power spectrum. This suggests that a measurement of the damping of the BAO signature might be a probe of the growth factor of the density fluctuations, though we need to further investigate if the effects of the redshift-space distortion or the galaxy clustering bias are influential to the damping.

This paper is organized as follows; In section 2, we briefly review the third order perturbation theory, and derive the second order power spectrum. In this formalism, the nonlinear gravitational clustering is described by the coupling of the Fourier modes of the density fluctuations and the peculiar velocity divergences. In section 3, we investigate the damping of the BAO signature due to the coupling of the Fourier modes in an analytic way. And a fitting formula of the damping, applicable in weakly nonlinear regime, is developed. The formula is compared with a result of  $N$ -body simulation. Extensions of the formula are also discussed. In section 4, with the use of the fitting formula, we demonstrate a future feasibility of constraining the growth factor through a measurement of the damping of the BAO signature. The last section is devoted to a summary and conclusions. Throughout this paper, we use the unit in which the velocity

of light equals 1, and adopt the Hubble parameter  $H_0 = 100h\text{km/s/Mpc}$  with  $h = 0.7$ , unless explicitly stated.

## 2. Quasi-nonlinear evolution of the matter power spectrum

To investigate the effect of the nonlinear gravitational clustering in the present work, we employ the standard perturbation theory (SPT) of the density fluctuations and the peculiar velocity divergences [28, 29, 30, 31, 32, 33, 34, 35, 36]. Numerical simulation is a rigorous approach to the gravitational clustering, but the perturbative approach has an advantage to understand which factors are relevant to the damping of the BAO signature in an analytic way. Recently, several authors have developed new formalism beyond the SPT [37, 38, 39, 40, 41, 42, 43, 44, 45, 46]. In the later subsection 3.3, we discuss a possible extension of our main result to include these formalism. However, let us start with briefly reviewing the derivation of the second order power spectrum on the basis of the SPT up to the third order of perturbations.

We consider the matter fluctuations after the recombination whose wavelength of interest is smaller than the horizon size, then the evolution of the matter fluctuations can be analyzed by the pressure-less nonrelativistic fluid with the Newtonian gravity. Denoting the comoving coordinates by  $\mathbf{x}$ , and the conformal time by  $\eta$ , the evolution equations are

$$\dot{\delta}(\mathbf{x}, \eta) + \nabla \cdot [(1 + \delta(\mathbf{x}, \eta)) \mathbf{v}(\mathbf{x}, \eta)] = 0, \quad (1)$$

$$\dot{\mathbf{v}}(\mathbf{x}, \eta) + (\mathbf{v}(\mathbf{x}, \eta) \cdot \nabla) \mathbf{v}(\mathbf{x}, \eta) + \mathcal{H}(\eta) \mathbf{v}(\mathbf{x}, \eta) = -\nabla \phi(\mathbf{x}, \eta), \quad (2)$$

$$\nabla^2 \phi(\mathbf{x}, \eta) = \frac{3}{2} \mathcal{H}^2(\eta) \delta(\mathbf{x}, \eta), \quad (3)$$

where  $\delta$  is the density contrast,  $\mathbf{v}$  is the peculiar velocity,  $\phi$  is the gravitational potential,  $a$  is the scale factor, a dot denotes the derivative with respect to the conformal time, and  $\mathcal{H} = \dot{a}/a$ . Here, the Einstein-de Sitter universe is assumed.

We ignore the rotational mode of the velocity, since our interest is only the growing solution, and the rotational mode is the decaying solution in the expanding universe. Then, we introduce the velocity divergence,

$$\theta(\mathbf{x}, \eta) \equiv \nabla \cdot \mathbf{v}(\mathbf{x}, \eta). \quad (4)$$

It is convenient to analyze the perturbations in the Fourier space, and we define the Fourier coefficients as

$$\delta(\mathbf{x}, \eta) = \int \frac{d^3k}{(2\pi)^3} \delta(\mathbf{k}, \eta) e^{-i\mathbf{k} \cdot \mathbf{x}}, \quad (5)$$

$$\theta(\mathbf{x}, \eta) = \int \frac{d^3k}{(2\pi)^3} \theta(\mathbf{k}, \eta) e^{-i\mathbf{k} \cdot \mathbf{x}}. \quad (6)$$

Then, equations (1) - (3) yield

$$\dot{\delta}(\mathbf{k}, \eta) + \theta(\mathbf{k}, \eta) = - \int d^3k_1 \int d^3k_2 \delta^{(3)}(\mathbf{k}_1 + \mathbf{k}_2 - \mathbf{k}) \frac{\mathbf{k} \cdot \mathbf{k}_1}{k_1^2} \theta(\mathbf{k}_1, \eta) \delta(\mathbf{k}_2, \eta), \quad (7)$$

$$\begin{aligned} \dot{\theta}(\mathbf{k}, \eta) + \mathcal{H}(\eta)\theta(\mathbf{k}, \eta) + \frac{3}{2}\mathcal{H}^2(\eta)\delta(\mathbf{k}, \eta) = \\ - \int d^3k_1 \int d^3k_2 \delta^{(3)}(\mathbf{k}_1 + \mathbf{k}_2 - \mathbf{k}) \frac{k^2(\mathbf{k}_1 \cdot \mathbf{k}_2)}{2k_1^2 k_2^2} \theta(\mathbf{k}_1, \eta) \theta(\mathbf{k}_2, \eta), \end{aligned} \quad (8)$$

where  $\delta^{(3)}(\mathbf{k})$  denotes the Dirac's delta function. The right hand side of these equations describes the mode-couplings which govern the nonlinear evolution of the matter fluctuations.

To solve these coupled equations, we adopt the perturbative expansion as

$$\delta(\mathbf{k}, \eta) = \sum_{n=1}^{\infty} a^n(\eta) \delta_n(\mathbf{k}), \quad \theta(\mathbf{k}, \eta) = \mathcal{H}(\eta) \sum_{n=1}^{\infty} a^n(\eta) \theta_n(\mathbf{k}). \quad (9)$$

In general, the  $n$ -th order solution can be written as

$$\delta_n(\mathbf{k}) = \int d^3q_1 \cdots \int d^3q_n \delta^{(3)}\left(\sum_{i=1}^n \mathbf{q}_i - \mathbf{k}\right) F_n(\mathbf{q}_1, \dots, \mathbf{q}_n) \prod_{i=1}^n \delta_1(\mathbf{q}_i), \quad (10)$$

$$\theta_n(\mathbf{k}) = - \int d^3q_1 \cdots \int d^3q_n \delta^{(3)}\left(\sum_{i=1}^n \mathbf{q}_i - \mathbf{k}\right) G_n(\mathbf{q}_1, \dots, \mathbf{q}_n) \prod_{i=1}^n \delta_1(\mathbf{q}_i), \quad (11)$$

where  $F_n(\mathbf{q}_1, \dots, \mathbf{q}_n)$  and  $G_n(\mathbf{q}_1, \dots, \mathbf{q}_n)$  are defined as

$$\begin{aligned} F_n(\mathbf{q}_1, \dots, \mathbf{q}_n) = \sum_{m=1}^{n-1} \frac{G_m(\mathbf{q}_1, \dots, \mathbf{q}_m)}{(2n+3)(n-1)} \left[ (1+2n) \frac{\mathbf{k} \cdot \mathbf{k}_1}{k_1^2} F_{n-m}(\mathbf{q}_{m+1}, \dots, \mathbf{q}_n) \right. \\ \left. + \frac{k^2(\mathbf{k}_1 \cdot \mathbf{k}_2)}{k_1^2 k_2^2} G_{n-m}(\mathbf{q}_{m+1}, \dots, \mathbf{q}_n) \right], \end{aligned} \quad (12)$$

$$\begin{aligned} G_n(\mathbf{q}_1, \dots, \mathbf{q}_n) = \sum_{m=1}^{n-1} \frac{G_m(\mathbf{q}_1, \dots, \mathbf{q}_m)}{(2n+3)(n-1)} \left[ 3 \frac{\mathbf{k} \cdot \mathbf{k}_1}{k_1^2} F_{n-m}(\mathbf{q}_{m+1}, \dots, \mathbf{q}_n) \right. \\ \left. + n \frac{k^2(\mathbf{k}_1 \cdot \mathbf{k}_2)}{k_1^2 k_2^2} G_{n-m}(\mathbf{q}_{m+1}, \dots, \mathbf{q}_n) \right]. \end{aligned} \quad (13)$$

Assuming that the first order density perturbations described by  $\delta_1(\mathbf{k})$  is a Gaussian random field, we obtain the second order matter power spectrum

$$P_{\text{SPT}}(k, z) = D_1^2(z) P_{\text{lin}}(k) + D_1^4(z) P_2(k), \quad (14)$$

where  $P_{\text{lin}}(k)$  is the linear power spectrum given by

$$(2\pi)^3 \delta^{(3)}(\mathbf{k} + \mathbf{k}') P_{\text{lin}}(k) = \langle \delta_1(\mathbf{k}) \delta_1(\mathbf{k}') \rangle, \quad (15)$$

$D_1(z)$  is the linear growth factor, and  $P_2(k)$  is the second order contribution to the power spectrum, which is conventionally expressed as follows;

$$P_2(k) = P_{22}(k) + 2P_{13}(k). \quad (16)$$

Taking the 4-point correlations of  $\delta_1(\mathbf{k})$  into consideration, we obtain the explicit form of  $P_{22}(k)$  expressed as the integral of the square of the linear power spectrum,

$$P_{22}(k) = 2 \int d^3q P_{\text{lin}}(q) P_{\text{lin}}(|\mathbf{k} - \mathbf{q}|) [F_2^{\text{s}}(\mathbf{q}, \mathbf{k} - \mathbf{q})]^2, \quad (17)$$

where  $F_2^s(\mathbf{q}_1, \mathbf{q}_2)$  is symmetrized over its arguments. On the other hand,  $P_{13}(k)$  has the form slightly different with  $P_{22}(k)$ ,

$$2P_{13}(k) = 6P_{\text{lin}}(k) \int d^3q P_{\text{lin}}(q) F_3^s(\mathbf{q}, -\mathbf{q}, \mathbf{k}). \quad (18)$$

The solid curve in figure 1 shows typical behaviour of  $P_{22}(k)$  and  $2P_{13}(k)$ , where the cosmological parameters are  $h = 0.7$ ,  $\Omega_m = 0.28$ ,  $\Omega_b = 0.046$ ,  $n_s = 0.96$  and  $\sigma_8 = 0.82$ . We discuss further details of the typical behaviour of  $P_{22}(k)$  and  $2P_{13}(k)$  in the next section.

Originally, this perturbation expansion is consistently formulated in the Einstein de-Sitter universe. The result is extensively used for the other general cosmological model, with the corresponding growth factor normalized as  $D_1(z) = a(z)$  at  $a(z) \ll 1$ . We follow this prescription because the validity of the extensive use of the result is known, for example, in the literature [36, 47].

### 3. Damping of the BAO signature

In this section, we will examine the damping of the BAO signature due to the nonlinear gravitational clustering with employing the third order perturbation theory. The BAO signature in the matter power spectrum can be extracted as follows:

$$B(k, z) \equiv \frac{P(k, z)}{\tilde{P}(k, z)} - 1, \quad (19)$$

where  $P(k, z)$  is the matter power spectrum including the BAO signature, but  $\tilde{P}(k, z)$  is the matter power spectrum without the BAO, which is calculated using the no-wiggle transfer function in [48]. Hereafter, the quantity with the 'tilde' implies the quantity computed using the no-wiggle transfer function. Within the third order perturbation theory, we may write

$$\tilde{P}_{\text{SPT}}(k, z) = D_1^2(z)\tilde{P}_{\text{lin}}(k) + D_1^4(z)\tilde{P}_2(k), \quad (20)$$

where  $\tilde{P}_2(k)$  is

$$\tilde{P}_2(k) = \tilde{P}_{22}(k) + 2\tilde{P}_{13}(k), \quad (21)$$

and  $\tilde{P}_{22}(k)$  and  $\tilde{P}_{13}(k)$  are, respectively, defined by (17) and (18), but with the no-wiggle transfer function.

Figure 2 shows  $B_{\text{SPT}}^{\text{exact}}(k, z)$  as a function of the wavenumber  $k$  for several redshifts, which is obtained using the third order perturbation theory (see also below). Here, the spatially flat universe with the cold dark matter (CDM) and the cosmological constant  $\Lambda$  is assumed, where the cosmological parameters are the same as those of Figure 1. The oscillating behaviour of the curves is the BAO signature. As the redshift becomes small, one can see that the amplitude of the oscillations decreases. This damping of the oscillations is more significant as  $k$  is larger.

### 3.1. Analytic approach

The aim of this paper is to understand the nature of the damping of the BAO signature in detail. To this end, the analytic approach based on the third order perturbation theory is useful. With the use of the formula of the second order power spectra, (14) and (20), we have

$$B_{\text{SPT}}^{\text{exact}}(k, z) = \frac{P_{\text{SPT}}(k, z)}{\tilde{P}_{\text{SPT}}(k, z)} - 1 = \frac{P_{\text{lin}}(k) + D_1^2(z)P_2(k)}{\tilde{P}_{\text{lin}}(k) + D_1^2(z)\tilde{P}_2(k)} - 1. \quad (22)$$

First, we adopt an approximation,

$$P_2(k) \simeq \tilde{P}_{22}(k) + 2P_{13}(k). \quad (23)$$

In brief,  $P_{22}(k)$  in (16) is replaced with  $\tilde{P}_{22}(k)$ . The validity of this approximation is demonstrated in figure 1, where the upper solid curve is  $P_{22}(k)$ , and the upper dotted curve is  $\tilde{P}_{22}(k)$ . The validity of this approximation comes from the fact that the mode-coupling of different Fourier modes decrease the coherent BAO signature. As shown in this figure, the tiny oscillatory feature remains. This may induce somewhat the small shift of the peaks(troughs) of the BAO, as mentioned in the reference [41]. However, this shift of peak location would not be problematic, as long as we are interested in the damping of the BAO signature.

On the other hand,  $P_{13}(k)$  can not be simply replaced with  $\tilde{P}_{13}(k)$ . However, careful consideration leads to an expression for  $\tilde{P}_{13}(k)$  in terms of the linear power spectrum multiplied by a monotonically decreasing function, as follows. First, we define

$$B_{\text{lin}}(k) \equiv \frac{P_{\text{lin}}(k)}{\tilde{P}_{\text{lin}}(k)} - 1, \quad (24)$$

which corresponds to (22), within the linear theory of density fluctuations. Note that  $B_{\text{lin}}(k)$  is not time-dependent. With this definition, we obtain

$$2P_{13}(k) = 6\tilde{P}_{\text{lin}}(k) [1 + B_{\text{lin}}(k)] \int d^3q P_{\text{lin}}(q) F_3^s(\mathbf{q}, -\mathbf{q}, \mathbf{k}). \quad (25)$$

Here, we apply the following approximation to the linear power spectrum of the integrand,

$$\begin{aligned} 2P_{13}(k) &\simeq 6\tilde{P}_{\text{lin}}(k) [1 + B_{\text{lin}}(k)] \int d^3q \tilde{P}_{\text{lin}}(q) F_3^s(\mathbf{q}, -\mathbf{q}, \mathbf{k}) \\ &= 2 [1 + B_{\text{lin}}(k)] \tilde{P}_{13}(k). \end{aligned} \quad (26)$$

Substituting (26) into (23),  $P_2(k)$  is written as

$$P_2(k) = \tilde{P}_2(k) + 2B_{\text{lin}}(k)\tilde{P}_{13}(k). \quad (27)$$

Then, from (22), we obtain

$$B_{\text{SPT}}^{\text{exact}}(k, z) \simeq \frac{1 + D_1^2(z) \frac{2\tilde{P}_{13}(k)}{\tilde{P}_{\text{lin}}(k)}}{1 + D_1^2(z) \frac{\tilde{P}_2(k)}{\tilde{P}_{\text{lin}}(k)}} B_{\text{lin}}(k). \quad (28)$$

This formula indicates how the BAO signature is modified as the gravitational clustering evolves, which is expressed by the BAO signature in the linear theory multiplied by the correction determined by the no-wiggle quantities and the growth factor. The second term of the denominator in (28) is small within the perturbation scheme, we may expand it as

$$B_{\text{SPT}}^{\text{exact}}(k, z) \simeq \left[ 1 - D_1^2(z) \frac{\tilde{P}_{22}(k)}{\tilde{P}_{\text{lin}}(k)} \left\{ 1 - D_1^2(z) \frac{\tilde{P}_2(k)}{\tilde{P}_{\text{lin}}(k)} + D_1^4(z) \left( \frac{\tilde{P}_2(k)}{\tilde{P}_{\text{lin}}(k)} \right)^2 - \dots \right\} \right] B_{\text{lin}}(k), \quad (29)$$

though the higher order terms make no sense because we are working in the second order theory of the power spectrum. The expression (29) indicates that the leading effect of the nonlinear mode-coupling on the damping is described by the factor  $-D_1^2(z)\tilde{P}_{22}(k)/\tilde{P}_{\text{lin}}(k)$ , and that the sign of the term clearly shows that this effect is a damping.

### 3.2. Fitting formula

As we are working within the third order perturbation theory, its prediction does not perfectly coincide with the result of full order computation, which can be obtained by  $N$ -body simulations. However, we believe that the prediction of the third order perturbation theory is useful in constructing a semi-analytic formula which reproduces the result of  $N$ -body simulations. Then, we here find a simple fitting formula which reproduces the prediction of the third order perturbation theory. We discuss the validity of the formula in comparison with a  $N$ -body simulation in the below.

Up to the second order of  $D_1(z)$ , (29) yields

$$B_{\text{SPT}}^{\text{exact}}(k, z) \simeq \left[ 1 - D_1^2(z) \frac{\tilde{P}_{22}(k)}{\tilde{P}_{\text{lin}}(k)} \right] B_{\text{lin}}(k). \quad (30)$$

From a detailed analysis of  $\tilde{P}_{22}(k)/\tilde{P}_{\text{lin}}(k)$  as a function of  $k$ , we find that the following fitting formula works well,

$$\frac{\tilde{P}_{22}(k)}{\tilde{P}_{\text{lin}}(k)} = \sigma_8^2 \left( \frac{k}{k_n} \right)^2 \left( 1 - \frac{\gamma}{k} \right), \quad (31)$$

where  $\sigma_8$  is the rms matter density fluctuations averaged over the sphere with the radius of  $8h^{-1}\text{Mpc}$ ,  $k_n$  and  $\gamma$  are the constant parameters which depend on  $\Omega_m h^2$ ,  $\Omega_b h^2$  and  $n_s$ . Figures 3 and 4 show the best-fit value of  $k_n$  and  $\gamma$  as a function of  $\Omega_m h^2$  and  $\Omega_b h^2$ , where we fixed  $n_s = 0.96$ . This shows that these two parameters depend on  $\Omega_m h^2$  and  $\Omega_b h^2$  linearly. We can show a similar dependence on  $n_s$ . Then, we found the following fitting formula:

$$k_n = -1.03(\Omega_m h^2 + 0.077)(\Omega_b h^2 - 0.24)(n_s + 0.92) \text{ hMpc}^{-1}, \quad (32)$$

$$\gamma = -11.4(\Omega_m h^2 - 0.050)(\Omega_b h^2 - 0.076)(n_s - 0.34) \text{ hMpc}^{-1}. \quad (33)$$

Though these dependence on the cosmological parameter might have to be investigated more carefully, but the validity is guaranteed in the following narrow range

$$0.13 \lesssim \Omega_m h^2 \lesssim 0.15, \quad (34)$$

$$0.022 \lesssim \Omega_b h^2 \lesssim 0.024, \quad (35)$$

$$0.94 \lesssim n_s \lesssim 0.98. \quad (36)$$

In the present paper, we simply assume that the dependence on the other cosmological parameters except for  $\Omega_m h^2$ ,  $\Omega_b h^2$  and  $n_s$  can be ignored.

Finally, we obtain the heuristic expression of the leading correction for the BAO signature,

$$B_{\text{SPT}}^{\text{fit}}(k, z) = \left[ 1 - f(\Omega_m h^2, \Omega_b h^2, n_s, \sigma_8, k, z) \right] B_{\text{lin}}(k), \quad (37)$$

with

$$f(\Omega_m h^2, \Omega_b h^2, n_s, \sigma_8, k, z) = \sigma_8^2 D_1^2(z) \left( \frac{k}{k_n} \right)^2 \left( 1 - \frac{\gamma}{k} \right). \quad (38)$$

Figure 5 demonstrates the agreement between this fitting formula,  $B_{\text{SPT}}^{\text{fit}}$ , and the prediction of the third order perturbation theory,  $B_{\text{SPT}}^{\text{exact}}$ , (22). As one can see from this figure, the agreement becomes worse as the redshift is lower and the wavenumber is larger. Figure 6 shows the relative error of the fitting formula,  $|B_{\text{SPT}}^{\text{fit}} - B_{\text{SPT}}^{\text{exact}}|/|B_{\text{SPT}}^{\text{exact}}|$ , as a function of the redshift at the wavenumbers of P1, P2, P3, T1, T2 and T3, which are defined in Figure 5. The relative error is about less than 10 % at worst in the range of the wavenumber  $k \lesssim 0.2 \text{ hMpc}^{-1}$  until  $z \sim 1$ . The sign of  $B_{\text{SPT}}^{\text{fit}} - B_{\text{SPT}}^{\text{exact}}$  of the third peak (trough) changes around the redshift 2.7 (1.4), where the relative error becomes zero. For the redshift less than 1, the agreement becomes worse especially at the large wavenumber  $k (\gtrsim 0.2 \text{ hMpc}^{-1})$ . However, we should also note that the third order perturbation theory becomes worse to reproduce  $N$ -body simulations for lower redshift and for larger wavenumbers.

Figure 7 shows a comparison of our fitting formula ( $B_{\text{SPT}}^{\text{fit}}$ , solid curve) and a result of  $N$ -body simulation (squares with error bar) [49]. This demonstrates that our fitting formula reproduces the result of  $N$ -body simulation for  $k \lesssim 0.2 \text{ hMpc}^{-1}$  until  $z \sim 1$  within error bars, roughly. In this conclusion, note that we focus on the damping of the BAO signature, not on the amplitude of the power spectrum itself.

In the  $N$ -body simulation, we adopt a  $\Lambda$ CDM cosmology ( $\Omega_m = 0.279$ ,  $\Omega_\Lambda = 0.721$ ,  $\Omega_b/\Omega_m = 0.165$ ,  $h = 0.701$ ,  $n_s = 0.96$ ,  $\sigma_8 = 0.817$ ; WMAP5 best fit value, [50]), and calculate the linear matter power spectrum using **CAMB** [51]. We adopt  $512^3$  particles in periodic cubes with each side  $1000h^{-1}\text{Mpc}$ , and displace  $N$ -body particles using the second-order Lagrangian perturbation theory (e.g., [52]) from uniform grid positions at  $z = 31$ . The simulations are carried out using the **Gadget2** code [53] to output data of 4 redshifts ( $z = 3, 2, 1$ , and  $0.5$ ). Our total simulation volume is  $8h^{-3}\text{Gpc}^3$ , which might be small to investigate our scales of interest (first a few BAO peaks). Then we correct the deviations from the ideal case of infinite volume, as follows.

In addition to the time integration using `Gadget2`, we also calculate the time evolution of the density contrast using the second-order perturbation theory starting from the identical initial condition with that used for the  $N$ -body simulation. We then calculate the power spectrum from the result of the perturbation theory, and measure the *deviation* from the the linear power spectrum at each output time. The deviation of our finite volume simulation is well explained by the mode-couplings predicted by the second-order perturbation theory. Then, we can obtain a corrected power spectrum by multiplying the measured power spectrum from  $N$ -body simulations by the ratio of the linear power spectrum to the power spectrum predicted by the perturbation theory. Thus the error bars in the figure stand for the remaining standard errors after this correction, which are very small compared with the usual cases in the region of the small wavenumbers. This is because the perturbation theory used for the correction is more accurate at the small wavenumbers, which can remove the deviations from the linear power spectrum better. This correction does not improve the errors at large wavenumbers (see [24], [49] for more details). Moreover, in order to construct the no-wiggle spectrum required for computing the ratio  $B$ , we use a cubic basis-spline fitting with the same break points as in [27] (see also [8]).

### 3.3. Possible extension and discussion

There are other possible effects which may affect the damping of the BAO signature: the higher order nonlinear effect, the redshift-space distortions and the clustering bias. These effects may be influential to the damping of the BAO signature, however, there remains a lot of uncertainties about these effects, at present. Here, let us consider a possible extension of our work to include the higher order nonlinear corrections in real space.

The standard perturbation theory is useful to analyse the damping of the BAO signature in an analytic way, however, it is not enough for precise predictions that match with result of  $N$ -body simulations in the regime where the nonlinear effect becomes significant. Recently, several authors have developed non-perturbative approach to the nonlinear density clustering, as mentioned above [37, 38, 39, 40, 41, 42, 43, 44, 45, 46].

As an alternative to the SPT, we here consider the work proposed by [46], which uses the technique of resumming infinite series of higher order perturbations on the basis of the Lagrangian perturbation theory (LPT). One of the advantage of this approach is the simplicity of the resulting expression of the nonlinear power spectrum, which enable us to incorporate the result into our formula. In the framework of the LPT[46], the matter power spectrum can be given by

$$P_{\text{LPT}}(k, z) = e^{-D_1(z)^2 g(k)} [D_1(z)^2 P_{\text{lin}}(k) + D_1(z)^4 P_2(k) + D_1(z)^4 P_{\text{lin}}(k) g(k)], \quad (39)$$

where

$$g(k) = \frac{k^2}{6\pi^2} \int dq P_{\text{lin}}(q). \quad (40)$$

Corresponding to (22), we define the BAO signature of the matter power spectrum based on the LPT,

$$B_{\text{LPT}}^{\text{exact}}(k, z) = \frac{P_{\text{LPT}}(k, z)}{\tilde{P}_{\text{LPT}}(k, z)} - 1, \quad (41)$$

where  $\tilde{P}_{\text{LPT}}(k, z)$  is defined by (39) but with the no-wiggle transfer function. Adopting an approximation,  $g(k) \simeq \tilde{g}(k)$ , we can obtain the following expression

$$B_{\text{LPT}}^{\text{exact}}(k, z) \simeq \frac{1 + \frac{D_1^2(z)}{1 + D_1^2(z)\tilde{g}(k)} \frac{2\tilde{P}_{13}(k)}{\tilde{P}_{\text{lin}}(k)}}{1 + \frac{D_1^2(z)}{1 + D_1^2(z)\tilde{g}(k)} \frac{\tilde{P}_2(k)}{\tilde{P}_{\text{lin}}(k)}} B_{\text{lin}}(k). \quad (42)$$

Repeating the same procedure from (28) to (30), one can obtain the leading correction to the BAO

$$B_{\text{LPT}}^{\text{exact}}(k, z) \simeq \left[ 1 - \frac{D_1^2(z)}{1 + D_1^2(z)\tilde{g}(k)} \frac{\tilde{P}_{22}(k)}{\tilde{P}_{\text{lin}}(k)} \right] B_{\text{lin}}(k), \quad (43)$$

then we obtain

$$B_{\text{LPT}}^{\text{fit}}(k, z) = \left[ 1 - \frac{f(\Omega_m h^2, \Omega_b h^2, n_s, \sigma_8, k, z)}{1 + D_1^2(z)\tilde{g}(k)} \right] B_{\text{lin}}(k), \quad (44)$$

as an extended fitting formula. Note that this reduces to the expression (30) in the limit of  $\tilde{g}(k) \rightarrow 0$ . Comparing (44) and (37), the difference is the contribution from  $D_1^2(z)\tilde{g}(k)$  in the denominator in front of  $\tilde{P}_{22}(k)/\tilde{P}_{\text{lin}}(k)$ . Since  $\tilde{g}(k)$  is positive, this correction make the damping of the BAO signature weaker compared with (37). In figure 7, the dashed curve plots  $B_{\text{LPT}}^{\text{fit}}(k, z)$ , (44).

In order to show the validity of the fitting formula, figure 8 plots the relative errors  $|\delta B/B| = |B_{\text{LPT}}^{\text{fit}} - B_{\text{LPT}}^{\text{exact}}|/|B_{\text{LPT}}^{\text{exact}}|$  at the wavenumber of the peaks and troughs as a function of the redshift, which is the same as Figure 6 but with the LPT instead of the SPT. As one can see from this figure, the fitting function  $B_{\text{LPT}}^{\text{fit}}$  better reproduces the damping of the BAO signature  $B_{\text{LPT}}^{\text{exact}}$ , compared with the case of the SPT, especially for larger wavenumber even at lower redshift. The relative error is less than 10 % in the range of the wavenumber  $k \lesssim 0.2 \text{ hMpc}^{-1}$  (near the third peak) until the present epoch,  $z = 0$ . In the below, we investigate other possible ways in describing the damping of the BAO signature due to the nonlinear effect.

One of the other possible formulas for the fitting function is the exponential function, as has been discussed in references (e.g., [7, 20, 22, 54]). Angulo *et al* [22] discussed the following fitting formula with the Gaussian damping function,

$$B(k, z) = \exp \left[ - \left( \frac{k}{\sqrt{2}k_*(z)} \right)^2 \right] B_{\text{lin}}(k, z), \quad (45)$$

where  $k_*(z)$  is a time-dependent free parameter, which should be calibrated by measurements from  $N$ -body simulations. This free parameter describes the time-dependence of the BAO damping, and Sanchez *et al* [54] obtained the best fit value,

$k_*(z) = 0.172 \text{ hMpc}^{-1}$  at  $z = 1$ , from their result of  $N$ -body simulations in [21]. Their model includes another parameter,  $\alpha$ , which describes the shift of the BAO scale in the wavenumber. However, in the present paper, we adopt the case of no shift of the BAO scale ( $\alpha = 1$ ) because our interest is focused on the damping of the BAO signature not on the shift of the BAO scale. It is also shown that  $\alpha$  almost equals 1 [21].

Figure 9 compares our fitting functions and the Gaussian damping function. The vertical axis stands for  $B^{\text{fit}}(k, z = 1)$  divided by  $B_{\text{lin}}(k, z = 1)$ , which means the damping function. The dotted curve and the solid curve are  $B_{\text{SPT}}^{\text{fit}}$  and  $B_{\text{LPT}}^{\text{fit}}$ , respectively. The dashed curve is the Gaussian damping function, (45), with  $k_*(z) = 0.172 \text{ hMpc}^{-1}$ .  $B_{\text{SPT}}^{\text{fit}}$  becomes negative as the wavenumber becomes larger,  $k \gtrsim 0.25 \text{ hMpc}^{-1}$ . This is because the phase inversion of the BAO signature appears in the SPT, as shown in the panel of  $z = 1$  in Figure 5, where of the SPT breaks down in this regime as mentioned in Section 3.2. On the other hand, the damping function based on the LPT,  $B_{\text{LPT}}^{\text{fit}}/B_{\text{lin}}$ , shows the similar behavior as the Gaussian damping function, which approaches zero in the limit of  $k \rightarrow 0.7$ . This is due to the modification by the factor,  $1/[1 + D_1^2(z)\tilde{g}(k)]$ , in (44).  $B_{\text{LPT}}^{\text{fit}}/B_{\text{lin}}$  becomes negative for  $k \gtrsim 0.7 \text{ hMpc}^{-1}$  because of the same reason as that for  $B_{\text{SPT}}^{\text{fit}}/B_{\text{lin}}$ .

In figure 9, we also plot the following damping function (dot-dashed curve),

$$B_{\text{SPT}}^{\text{exp}}(k, z) = \exp \left[ -f(\Omega_m h^2, \Omega_b h^2, n_s, \sigma_8, k, z) \right] B_{\text{lin}}(k). \quad (46)$$

The leading term of the expansion of this damping function with respect to  $D_1^2(z)$  leads to  $B_{\text{SPT}}^{\text{fit}}$ , (37). As one can see, this damping function  $B_{\text{SPT}}^{\text{exp}}$  agrees with the Gaussian damping function, (45). This means that the higher order perturbations is important in describing the BAO signature for the regime of the wavenumber,  $k \gtrsim 0.2 \text{ hMpc}^{-1}$  at redshift 1.

The result of this section gives us a clue to find how to describe the BAO damping due to the nonlinear gravitational clustering. The BAO damping is determined by the normalization  $\sigma_8$  and the growth factor  $D_1(z)$ . This suggests that a measurement of the BAO damping might be useful to estimate the growth factor of the amplitude of the density perturbations,  $\sigma_8 D_1(z)$ . In section 4, we demonstrate a feasibility of constraining  $\sigma_8 D_1(z)$  by measuring the damping of the BAO signature.

#### 4. Feasibility of Constraining $\sigma_8 D_1(z)$

As shown in the previous section, the damping of the BAO signature is closely related with the amplitude of the power spectrum, which is determined by  $\sigma_8 D_1(z)$ , while the BAO signature within the linear theory is determined by the density parameters  $\Omega_m h^2$  and  $\Omega_b h^2$ . In this section, we discuss the feasibility of constraining  $\sigma_8 D_1(z)$  by measuring the damping of the BAO in the power spectrum in quasi-nonlinear regime. To this end, the formula developed in the previous section is useful.

As mentioned in section 1 and subsection 3.3, the redshift-space distortions and the clustering bias might be additionally influential to the damping of the BAO signature.

However, we here assume an optimistic case that the damping is determined by the quasi-nonlinear clustering effect and neglect the effects on the damping of the BAO signature from the redshift-space distortions and the clustering bias. Then, we study how a measurement of the damping is useful to determine  $\sigma_8 D_1(z)$ . Very recently, it is recognized that a measurement of the growth factor of the density perturbations is a key to distinguish between the dark energy model and modified gravity model for the cosmic accelerated expansion (e.g., [55, 56], and references therein). Our investigation is the first step to investigate if a measurement of the BAO damping is useful to measure the growth factor.

In our investigation, we adopt a simple Monte Carlo simulation of the galaxy power spectrum assuming the  $\Lambda$ CDM model. The error of the galaxy power spectrum depends on its amplitude. For definiteness, we assume the galaxy power spectrum  $P_{\text{gal}}(k, z)$  is modeled with the no-wiggle linear power spectrum in real space,  $\tilde{P}_{\text{lin}}(k, z)$ , as

$$P_{\text{gal}}(k, z) = [1 + B(k, z)]\tilde{P}_{\text{gal}}(k, z), \quad (47)$$

with

$$\tilde{P}_{\text{gal}}(k, z) = b^2 \frac{1 + Qk^2}{1 + A_1 k + A_2 k^2} \tilde{P}_{\text{lin}}(k, z), \quad (48)$$

where we use (44) as  $B(k, z)$ ,  $b$  is a constant bias factor, and  $A_1$ ,  $A_2$  and  $Q$  are the parameters, which describe the correction of the nonlinear clustering, the redshift-space distortions and the scale-dependent bias to the no-wiggle power spectrum. This model is based on the  $Q$ -model of Cole *et al* [57], and is elaborated by Sanchez *et al* [54] by adding the new parameter  $A_2 (= Q/10)$  which better reproduces the nonlinear power spectrum at large wavenumber. Cole *et al* [57] showed that, from numerical study, the value of  $A_1 = 1.4$  is adequate to reconstruct the galaxy power spectrum in redshift-space, though  $Q$  strongly depends on the galaxy type [57, 58, 59]. Then, for simplicity, we here adopt  $A_1 = 1.4$  and consider the cases  $Q = 4, 8, 16, 32$ , to estimate the error for the galaxy power spectrum. We assume the bias parameter  $b = 2$ , for simplicity.

To estimate the constraint on the growth factor, we perform a simple Monte-Carlo simulation. We assume that the BAO signature,  $B(k, z)$ , can be extracted from a galaxy power spectrum by the method like in the reference [5]. The variance of the error in measuring the BAO signature can be estimated by

$$\Delta B^2(k) = \frac{\Delta P_{\text{gal}}^2(k, z)}{[\tilde{P}_{\text{gal}}(k, z)]^2} \quad (49)$$

with

$$\Delta P_{\text{gal}}^2(k, z) = 2 \frac{(2\pi)^3}{\Delta V_k} \mathcal{Q}^2(k, z), \quad (50)$$

where  $\Delta V_k = 4\pi k^2 \Delta k$  is the volume of the shell in the Fourier space, and  $\mathcal{Q}^2(k, z)$  is defined as

$$\mathcal{Q}^{-2}(k, z) = \Delta A \int dz \frac{ds[z]}{dz} s^2[z] \frac{\bar{n}^2(s[z])}{[1 + \bar{n}(s[z])P_{\text{gal}}(k, s[z])]^2}, \quad (51)$$

where  $\bar{n}(s)$  is the comoving mean number density,  $s = s[z]$  is the comoving distance-redshift relation, and  $\Delta A$  is the survey area.

With the use of the above formulas, we assess  $\chi^2$  defined by

$$\chi^2 = \sum_i \frac{[B(k_i, z)^{th} - B(k_i, z)^{obs}]^2}{\Delta B^2(k_i, z)}, \quad (52)$$

where  $B(k_i, z)^{th}$  is the theoretical one of a fiducial target model at the wavenumber  $k_i$ , while  $B(k_i, z)^{obs}$  is the corresponding observational one. The fiducial target model is  $\Omega_m = 0.28$  and  $\sigma_8 = 0.82$ ,  $\Omega_b = 0.046$ ,  $h = 0.7$ , and  $n_s = 0.96$ , which are the same as those adopted in figure 1.  $B(k_i, z)^{obs}$  is obtained through a Monte Carlo simulation, following the steps in the below,

- (i) Based on the fiducial model, compute  $B(k_i, z)$  and the variance  $\Delta B(k_i, z)$  at  $k_i = \Delta k(i - 0.5)$ , for  $i = 4, 5, \dots, 19$ . Here we specify a bin of the Fourier space,  $\Delta k = 0.01 h \text{Mpc}^{-1}$ , and consider the range of  $0.03 < k < 0.19$ , where the validity of our formula in the previous section is guaranteed. We assume two galaxy redshift samples as typical future survey. One is the WFMOS-like sample,  $\Delta A = 2000 \text{ deg}^2$  in the range of redshift  $0.5 < z < 1.3$ , and  $\bar{n} = 5.0 \times 10^{-4} [h^{-1} \text{Mpc}]^{-3}$ , which contains  $2.1 \times 10^6$  galaxies. The other sample assumes the same number density and the range of the redshift, but the larger survey area  $\Delta A = 4\pi$  steradian.
- (ii) Each  $B(k_i, z)^{obs}$  is obtained through a random process assuming the Gaussian distribution function with the variance  $\Delta B^2(k_i, z)$ . The data points in figure 10 show an example of a set of  $B(k_i, z)^{obs}$  generated through the random process.
- (iii) We assess the values of  $\chi^2$  with this sample obtained by the step (i) and (ii).

We iterate these steps and compute 1000 sets of  $\chi^2$ , then obtain the average of  $\chi^2$ . For the theoretical model,  $B(k_i, z)^{th}$ , we fixed  $\Omega_b h^2$ ,  $h$ , and  $n_s$  as those of the fiducial model, but took  $\Omega_m h^2$  and  $\sigma_8 D_1(z = 0.9)$  as the variable parameters. Solid curves in figure 11 show the contour of  $\Delta\chi^2 = 2.3$  (inner curve) and  $\Delta\chi^2 = 6.17$  (outer curve), which corresponds to the  $1\sigma$  and the  $2\sigma$  statistical confidence level, respectively, in the  $\Omega_m h^2$  and  $\sigma_8 D_1(z = 0.9)$  plane, for the WFMOS-like galaxy sample of  $\Delta A = 2000 \text{ deg}^2$ . The dotted curves show the same but with the sample of the survey area  $\Delta A = 4\pi$  steradian.

From figure 11, one can read that the  $1\sigma$  error of  $\sigma_8 D_1(z = 0.9)$  is about 0.2 for the sample of  $\Delta A = 2000 \text{ deg}^2$ , and is about 0.05 for the sample of  $\Delta A = 4\pi$  steradian. Thus, the constraint on  $\sigma_8 D_1(z = 0.9)$  of the WFMOS-like sample ( $\Delta A = 2000 \text{ deg}^2$ ) is not very stringent. We already have the small uncertainty of  $\sigma_8 D_1(z = 0.9)$  at the level of a few  $\times 0.01$  [36], from the result by the WMAP observations, which is obtained on the basis of the flat CDM cosmological model with the cosmological constant. However, we note that the BAO damping is unique and independent to obtain a constraint on  $\sigma_8 D_1(z)$  around the redshift 1.

It would be useful to discuss the origin of the error. To this end, we adopt the Fisher matrix approach. As we are considering the constraint from the damping of the

BAO signature, we may work with the formula for the Fisher matrix

$$F_{ij} = \frac{1}{4\pi^2} \int_{k_{\min}}^{k_{\max}} dk k^2 \frac{\partial B(k, z)}{\partial \theta_i} \frac{\partial B(k, z)}{\partial \theta_j} \frac{\tilde{P}_{\text{gal}}^2(k, z)}{\mathcal{Q}^2(k, z)}, \quad (53)$$

where  $\theta_i$  denotes cosmological parameters, for which we focus on  $\sigma_8 D_1(z)$  and  $\Omega_m h^2$ ,  $\tilde{P}_{\text{gal}}(k, z)$  is defined by (48),  $\mathcal{Q}^2(k, z)$  is defined by (51), we adopt (44) as  $B(k, z)$ , and  $k_{\min} = 0.02 h \text{Mpc}^{-1}$  and  $k_{\max} = 0.2 h \text{Mpc}^{-1}$ . The minimum error attainable on  $\theta_i$  is expressed by the diagonal part of the inverse Fisher-matrix,  $\Delta \theta_i = F_{\theta_i \theta_i}^{-1/2}$ , if the other parameters are known. Figure 12 plots the errors  $\Delta(\sigma_8 D_1(z = 0.9))$  and  $\Delta(\Omega_m h^2)$ , obtained from the Fisher-matrix, as a function of the mean number density  $\bar{n}(b/2)^2$ .<sup>‡</sup> The thick (thin) solid curve is  $\Delta(\sigma_8 D_1(z = 0.9))$  of the sample with  $\Delta A = 2000 \text{ deg.}^2$  ( $\Delta A = 4\pi$  radian). The dotted curve is  $\Delta(\Omega_m h^2)$ . Here we adopted  $Q = 16$ , but the result is not sensitive to this choice. One can read that the value of the error at the point  $\bar{n}(b/2)^2 = 5 \times 10^{-4} [h^{-1} \text{Mpc}]^{-3}$  is consistent with the result of figure 11.

Figure 12 demonstrates that the constraint can be improved by increasing the number density of the galaxy sample, but can not be improved for  $\bar{n}(b/2)^2 \gtrsim 10^{-3} [h^{-1} \text{Mpc}]^{-3}$ . The reason can be explained using figure 13, which plots  $\bar{n} P_{\text{gal}}(k, z = 0.9)$  as a function of the wavenumber, where we fixed  $\bar{n}(b/2)^2 = 5 \times 10^{-4} [h^{-1} \text{Mpc}]^{-3}$ . In the region  $k < 0.2 h \text{Mpc}^{-1}$ , we have  $\bar{n} P_{\text{gal}}(k, z = 0.9) > 1$ , which means that the shotnoise is not the dominant component of the error. However, the constraint on the parameter is slightly improved by increasing the number density  $\bar{n}$ , depending on the bias  $b$ .

Finally in this section, we mention the effect of the redshift-space distortions and the clustering bias on the BAO damping, which might be influential in measuring  $\sigma_8 D_1(z)$ . It would be true that there still remains room to investigate how the redshift-space distortions and the clustering bias affect the BAO damping. If the effect of the redshift-space distortions and the clustering bias on the BAO damping could not be clarified, it would make it difficult to conclude that the BAO damping is useful. However, very recently, several authors have discussed the issue [54, 60, 61]. If the effect on the BAO damping are well understood, it can be a signal, and would be useful in measuring the growth factor.

## 5. Summary and Conclusions

In the present paper, we examined the effect of the nonlinear gravitational clustering on the BAO signature in the matter power spectrum. In particular, we focused on the damping of the BAO signature in the quasi-nonlinear regime. Our approach is based on the third order perturbation theory of the matter fluctuations, which enables us to investigate the damping in an analytic way. We found a simple analytic expression that describes the damping of the BAO signature, which clarifies what the important factor is

<sup>‡</sup> Note that the Fisher-matrix depends on the parameter  $\bar{n} b^2$ .

for the damping. We showed that the leading correction for the damping is in proportion to the combination of  $(\sigma_8 D_1(z))^2$ . On the basis of the result, we constructed a fitting formula for the correction of the damping of the BAO signature in the weakly nonlinear regime, which is expressed as a function of  $k$ ,  $\Omega_m h^2$ ,  $\Omega_b h^2$  and  $n_s$ . This fitting formula reproduces the damping of the BAO signature of the second order power spectrum within the standard perturbation theory at 10% level for  $k \lesssim 0.2 \text{ hMpc}^{-1}$  until  $z \sim 1$ , though the formula is only guaranteed in a narrow range of the parameters  $\Omega_m h^2$ ,  $\Omega_b h^2$  and  $n_s$ .

We also discussed a possible extension of our formula to elaborate higher order nonlinear corrections using a technique of resumming infinite series of higher order perturbations on the basis of the Lagrangian perturbation theory. This extended formula reproduces the damping of the BAO signature of the second order power spectrum based on the Lagrangian perturbation theory at 10% level for  $k \lesssim 0.2 \text{ hMpc}^{-1}$  until  $z \sim 0$ . This formula was compared with a result of  $N$ -body simulation, which showed the validity of the extended formula.

A measurement of the damping of the BAO signature might be useful as a probe of the growth factor of the density fluctuations. As a first step to investigate such the possibility, we assessed the feasibility of constraining  $\sigma_8 D_1(z)$  by measuring the damping of the BAO in the power spectrum. For a useful constraint, we need a very wide survey area of the sky. For a definite conclusion, however, we must include the effect of the redshift-space distortions and the galaxy clustering bias on the damping of the BAO signature. Thus, more sophisticated formula including the effect of the redshift-space distortions and the galaxy clustering bias at the same time is required. If this effect on the BAO damping was well understood, it can be useful in measuring the growth factor. We plan to revisit this issue in future work.

## Acknowledgments

We thank A. Taruya, T. Matsubara, Y. Suto and G. Hütsi for useful discussions and comments. We are also grateful to anonymous referee for useful comments which helped to improve the earlier version of the manuscript. T. N. is supported by a Grand-in-Aid for Japan Society for the Promotion of Science (JSPS) Fellows (DC1: 19-7066). This work is supported by Grant-in-Aid for Scientific research of Japanese Ministry of Education, Culture, Sports and Technology (Nos. 18540277, 19035007).

## References

- [1] Albrecht A *et al*, 2006 arXiv:astro-ph/0609591
- [2] Peacock J A *et al*, 2006 arXiv:astro-ph/0610906
- [3] Eisenstein D J *et al*, 2005 *Astrophys. J.* 633 560
- [4] Hütsi G, 2006 *Astron. Astrophys.* 449 891
- [5] Percival W J *et al*, 2007 *Astrophys. J.* 657 645
- [6] Percival W J *et al*, 2007 *Astrophys. J.* 657 51

- [7] Tegmark M *et al*, 2006 Phys. Rev. D 74 123507
- [8] Percival W J *et al*, 2007 Mon. Not. R. Astron. Soc. 381 1053
- [9] Okumura T *et al*, 2008 Astrophys. J. 677 889
- [10] Hüetsi G, 2006 Astron. Astrophys. 459 375
- [11] <http://www.sdss3.org/>
- [12] Totani T, 2006 private communication
- [13] Bassett B A, Nichol R C and Eisenstein D J (the WFMOS Feasibility Study Dark Energy Team), 2005 arXiv:astro-ph/0510272
- [14] <http://www.lsst.org/>
- [15] <http://www.skatelescope.org/>
- [16] Robberto M *et al*, 2007 arXiv:0710.3970
- [17] Seo H-J and Eisenstein D J, 2003 Astrophys. J. 598 720
- [18] Seo H-J and Eisenstein D J, 2005 Astrophys. J. 633 575
- [19] Seo H-J and Eisenstein D J, 2007 astro-ph/0701079
- [20] Seo H-J *et al*, 2008 arXiv:0805.0117
- [21] Angulo R *et al*, 2005 Mon. Not. R. Astron. Soc. Lett. 362 L25
- [22] Angulo R *et al*, 2008 Mon. Not. R. Astron. Soc. 383 755
- [23] Shoji M *et al*, 2008 arXiv:0805.4238
- [24] Takahashi R *et al*, 2008 arXiv:0802.1808
- [25] Wang Y, 2006 Astrophys. J. 647 1
- [26] McDonald P and Eisenstein D, 2007 Phys. Rev. D 76 063009
- [27] Nishimichi T *et al*, 2007 Publ. Astron. Soc. Japan 59 1049
- [28] Juszkiewicz R, 1981 Mon. Not. R. Astron. Soc. 197 931
- [29] Vishniac E T, 1983 Mon. Not. R. Astron. Soc. 203 345
- [30] Fry J N, 1984 Astrophys. J. 279 499
- [31] Goroff M H *et al*, 1986 Astrophys. J. 311 6
- [32] Makino N, Sasaki M and Suto Y, 1992 Phys. Rev. D 46 585
- [33] Jain B and Bertschinger E, 1994 Astrophys. J. 431 495
- [34] Bernardeau F, Colombi S, Gaztanaga E and Scoccimarro R, 2002 Phys. Rep. 367 1
- [35] Saito S, Takada M and Taruya A, 2008 Phys. Rev. Lett. 100 191301
- [36] Jeong D and Komatsu E, 2006 Astrophys. J. 651 619
- [37] Valageas P, 2004 Astron. Astrophys. 421 23
- [38] Valageas P, 2007 Astron. Astrophys. 465 725
- [39] Crocce M and Scoccimarro R, 2006 Phys. Rev. D 73 063519
- [40] Crocce M and Scoccimarro R, 2006 Phys. Rev. D 73 063520
- [41] Crocce M and Scoccimarro R, 2008 Phys. Rev. D 77 023533
- [42] McDonald P, 2007 Phys. Rev. D 75 043514
- [43] Matarrese S and Pietroni M, 2007 J. Cosmol. Astropart. Phys. JCAP06(2007)026
- [44] Izumi K and Soda J, 2007 Phys. Rev. D 76 083517
- [45] Taruya A and Hiramatsu T, 2007 arXiv:0708.1367
- [46] Matsubara T, 2008 Phys. Rev. D 77 063530
- [47] Bernardeau F, 1994 Astrophys. J. 433 1
- [48] Eisenstein D J and Hu W, 1998 Astrophys. J. 496 605
- [49] Nishimichi T *et al*, 2008 arXiv:0810.0813
- [50] Komatsu E *et al*, 2008 arXiv:0803.0547
- [51] Lewis A *et al*, 2000 Astrophys. J. 538 473
- [52] Crocce M *et al*, 2006 Mon. Not. R. Astron. Soc. 373 369
- [53] Springel V, 2005 Mon. Not. R. Astron. Soc. 364 1105
- [54] Sanchez A G *et al*, 2008 arXiv:0804.0233
- [55] Yamamoto K *et al*, 2007 Phys. Rev. D 76 023504
- [56] Yamamoto K, Sato T and Hütsi G, 2008 Prog. Theor. Phys. 120 609

- [57] Cole S *et al*, 2005 Mon. Not. R. Astron. Soc. 362 505
- [58] Sanchez A G and Cole S, 2008 Mon. Not. R. Astron. Soc. 385 830
- [59] Hamann J *et al*, 2008 J. Cosmol. Astropart. Phys. JCAP07(2008)017
- [60] Matsubara T, 2008 arXiv:0807.1733
- [61] Jeong D and Komatsu E, 2008 arXiv:0805.2632

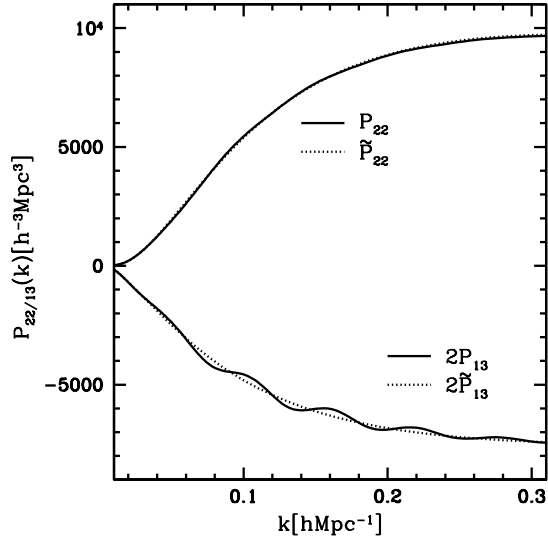


**Figure 1.** Typical behavior of  $P_{22}(k)$  (upper solid curve) and  $2P_{13}(k)$  (lower solid curve), which are calculated using the transfer function suggested by [48] with the BAO. The cosmological parameters are  $h = 0.7$ ,  $\Omega_m = 0.28$ ,  $\Omega_b = 0.046$ ,  $n_s = 0.96$  and  $\sigma_8 = 0.82$ . The dotted curves show  $\tilde{P}_{22}(k)$  (upper curve) and  $2\tilde{P}_{13}(k)$  (lower curve).

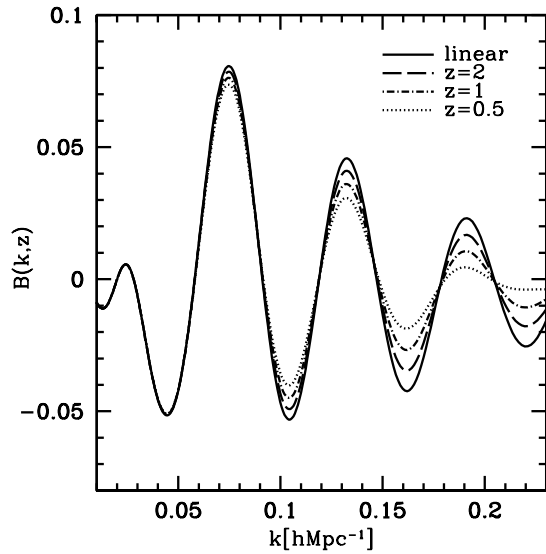


**Figure 2.**  $B_{\text{SPT}}^{\text{exact}}(k, z)$  as a function of  $k$  for several redshifts,  $z = 2, 1, 0.5$ , which are derived from the matter power spectrum including the second order contributions. The solid curve is the linear theory. The cosmological parameters are the same as those of figure 1. One can see the damping of the amplitude of the BAO as the redshift becomes small. In addition, this damping is more significant as the wavenumber  $k$  is larger.

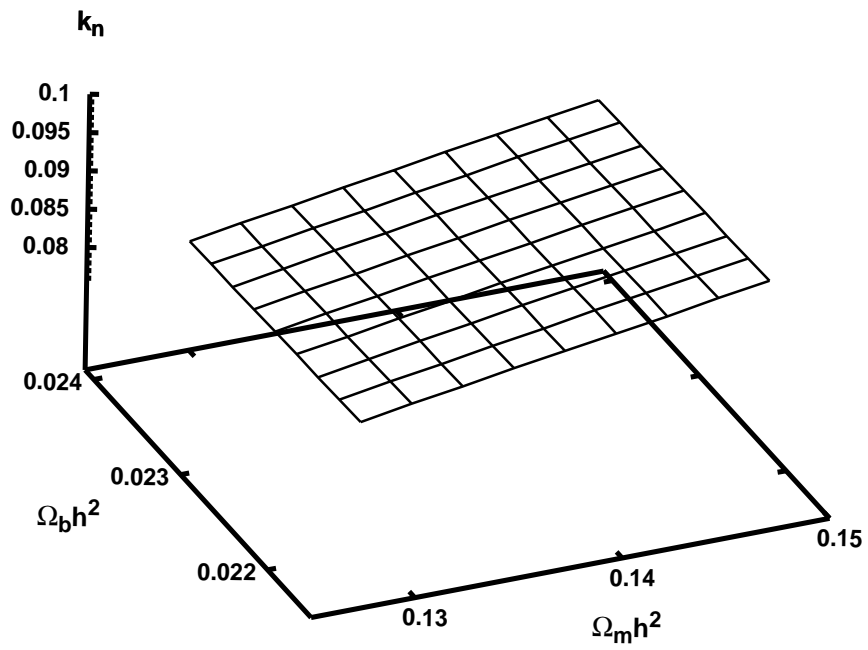


**Figure 3.** The best-fit  $k_n$  as a function of  $\Omega_m h^2$  and  $\Omega_b h^2$ . The other cosmological parameters are the same as those of figure 1.

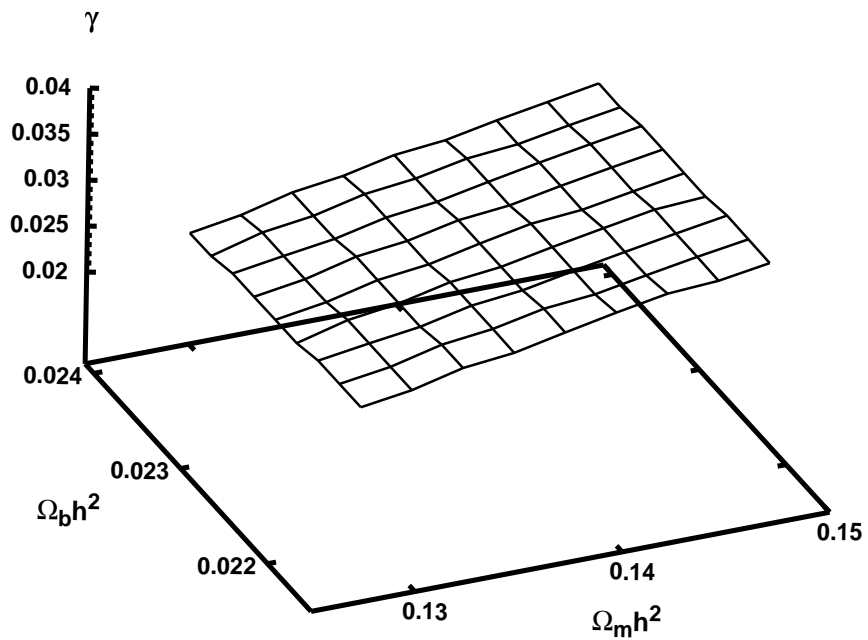


**Figure 4.** The best-fit  $\gamma$  as a function of  $\Omega_m h^2$  and  $\Omega_b h^2$ . The other cosmological parameters are the same as those of figure 1.

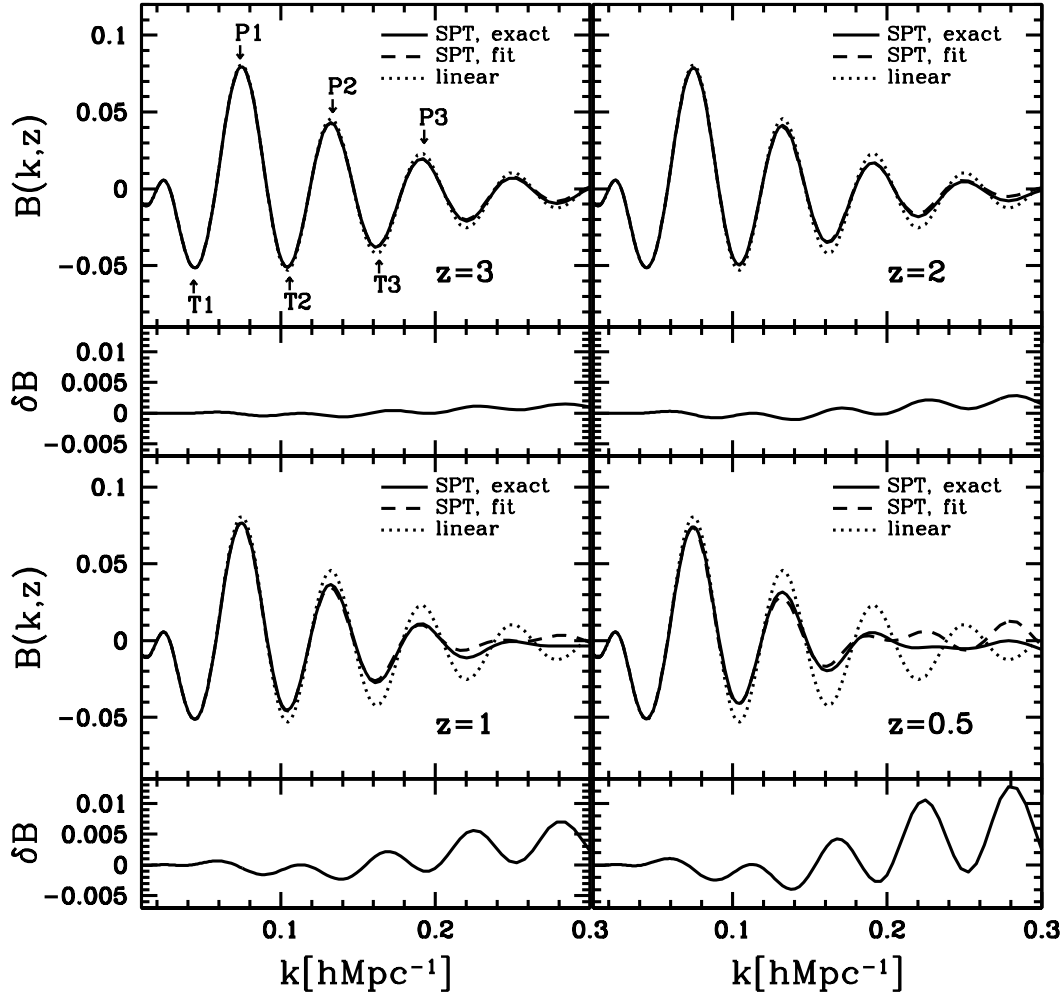


**Figure 5.** This figure compares our fitting formula ( $B_{SPT}^{\text{fit}}$ , dashed curve), (37), and the formula of the third order perturbation ( $B_{SPT}^{\text{exact}}$ , solid curve), (22), for various redshifts ( $z=3, 2, 1, 0.5$ ). The dotted curve is the linear theory.  $\delta B$  is the relative difference between the solid curve and the dotted curve ( $\delta B = B_{SPT}^{\text{fit}} - B_{SPT}^{\text{exact}}$ ). Here, the cosmological parameters are the same as those of Figure 1. P1, P2 and P3 (T1, T2 and T3) denote the first, the second and the third peak (trough), respectively, used in Figure 6.

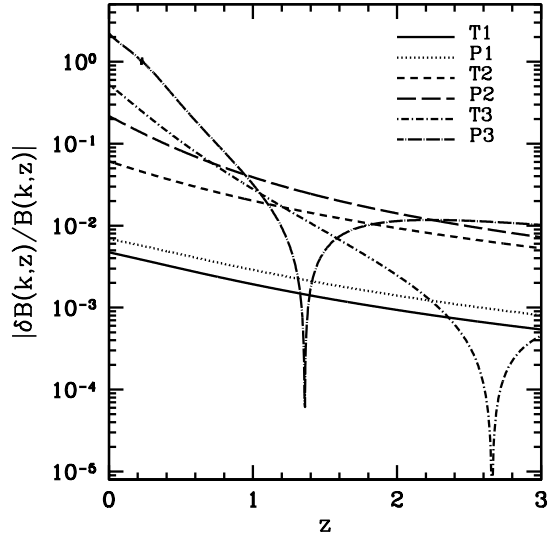


**Figure 6.** Relative error  $|\delta B/B| = |B_{\text{SPT}}^{\text{fit}} - B_{\text{SPT}}^{\text{exact}}|/|B_{\text{SPT}}^{\text{exact}}|$  as a function of the redshift at the wavenumber of P1, P2, P3, T1, T2 and T3, respectively, defined in Figure 5.

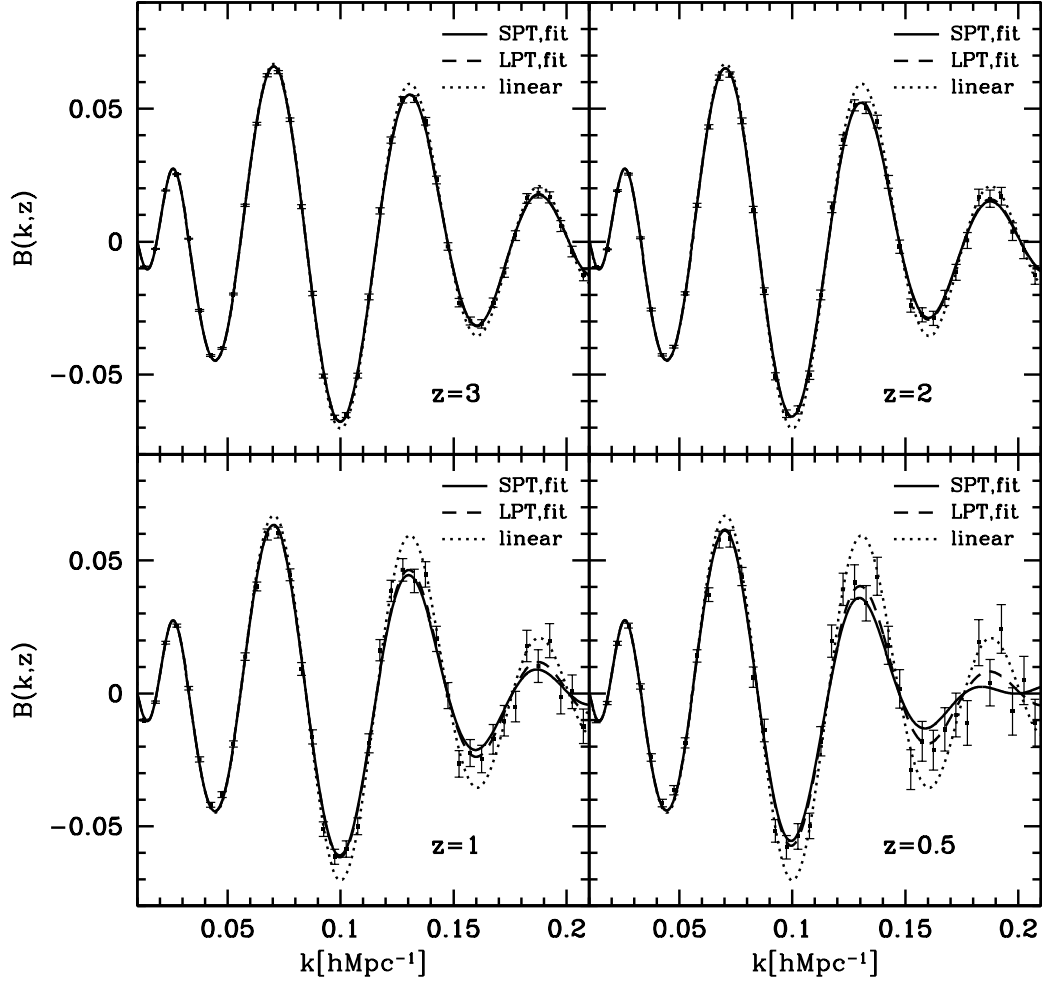


**Figure 7.** The square with the error bar is the result of  $N$ -body simulation. The solid curve is the fitting formula based on the SPT,  $B_{\text{SPT}}^{\text{fit}}$  of (37), while the dotted curve is the linear theory. The dashed curve is the result of an extended fitting formula,  $B_{\text{LPT}}^{\text{fit}}$  of (44). The degree of the damping of  $B_{\text{LPT}}^{\text{fit}}$ , is slightly weaker than that of  $B_{\text{SPT}}^{\text{fit}}$ .

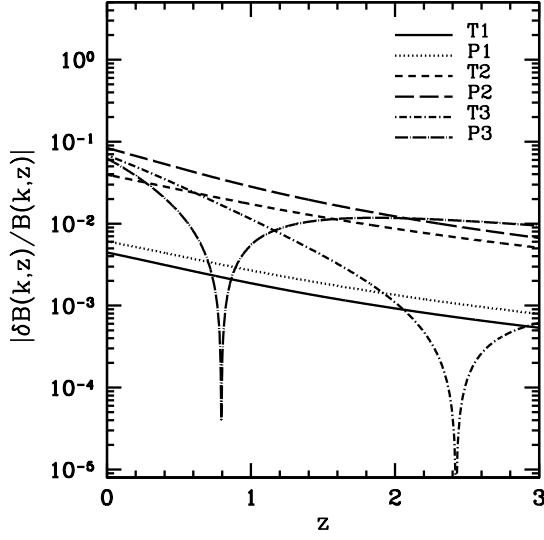


**Figure 8.** Same as Figure 6 but with the LPT instead of the SPT. Relative error is  $|\delta B/B| = |B_{\text{LPT}}^{\text{fit}} - B_{\text{LPT}}^{\text{exact}}|/|B_{\text{LPT}}^{\text{exact}}|$ .

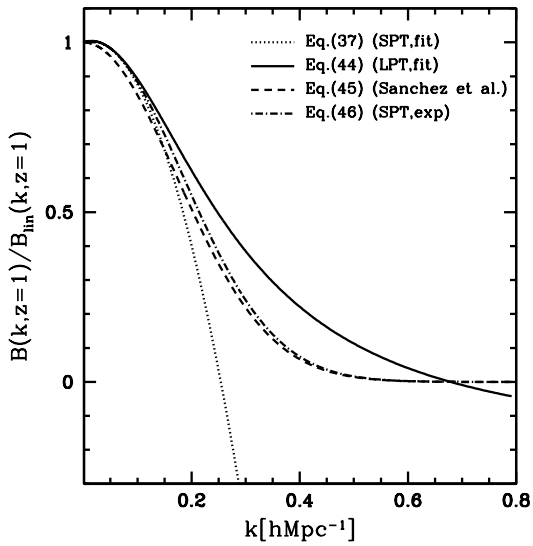


**Figure 9.** Comparison of fitting functions of the damping. The dotted curve is  $B_{\text{SPT}}^{\text{fit}}$ , (37), while the solid curve is  $B_{\text{LPT}}^{\text{fit}}$ , (44). The dashed curve is the Gaussian damping function, (45), with  $k_*(z) = 0.172 h\text{Mpc}^{-1}$ . The dot-dashed curve is  $B_{\text{SPT}}^{\text{exp}}$ , (46). In this plot, we adopted the same cosmological parameters as those in [54].

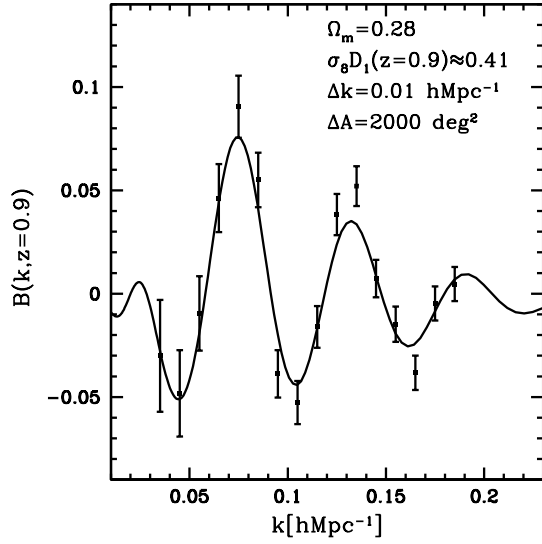


**Figure 10.** The solid curve is the prediction of the fiducial model, whose parameters are the same as those of figure 1, while the squares with the error bar is an example of  $B^{\text{obs}}(k_i, z = 0.9)$ , obtained through our Monte Carlo simulation. For the galaxy sample, we assumed the WFMOS-like sample of the comoving mean number density  $\bar{n} = 5.0 \times 10^{-4} [h^{-1}\text{Mpc}]^{-3}$  and the survey area  $2000 \text{ deg}^2$  in the range of redshift  $0.5 < z < 1.3$ . The bin size of the Fourier space is  $\Delta k = 0.01 \text{ hMpc}^{-1}$ .

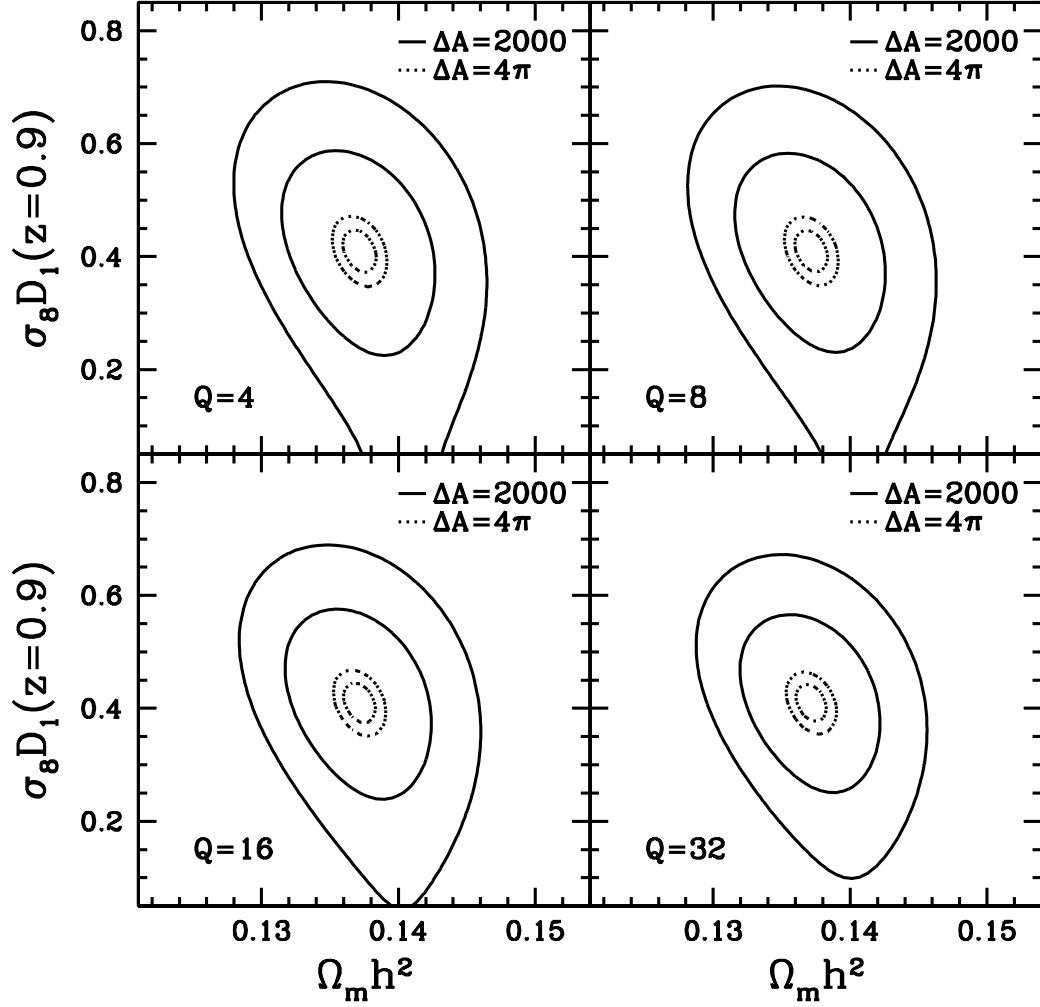


**Figure 11.** Contours of  $\Delta\chi^2$  in  $\Omega_m h^2$  and  $\sigma_8 D_1(z = 0.9)$  plane. The solid curves assume the WFMOS-like sample of the survey area,  $\Delta A = 2000$  deg<sup>2</sup>. Inner (outer) curve is the contour of  $\Delta\chi^2 = 2.3$  ( $\Delta\chi^2 = 6.17$ ), which corresponds to  $1\sigma$  ( $2\sigma$ ) confidence level. The dotted curve is the same as the solid curve, but assumes the survey area,  $\Delta A = 4\pi$  steradian.

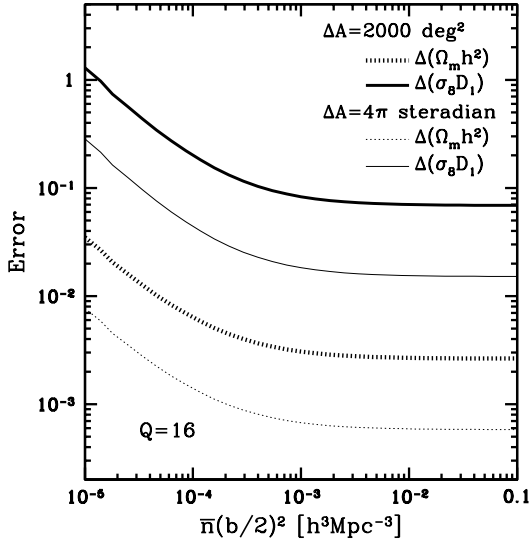


**Figure 12.** The  $1\sigma$ -level statistical errors of  $\Omega_m h^2$  (solid curve) and  $\sigma_8 D_1(z = 0.9)$  (dotted line) as a function of the number density  $\bar{n}(b/2)^2$ . The thick curves assume  $\Delta A = 2000 \text{ deg}^2$ , and the thin curves assume  $\Delta = 4\pi \text{ steradian}$ . In this figure, we fixed  $Q = 16$ .

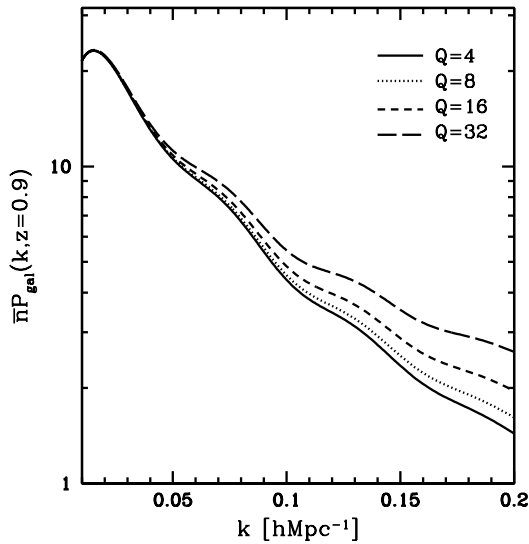


**Figure 13.** The galaxy power spectrum multiplied by the mean number density,  $\bar{n}P_{\text{gal}}(k, z = 0.9)$ , as a function of  $k$ . Here, we fixed  $\bar{n}(b/2)^2 = 5 \times 10^{-4} [h^{-1} \text{Mpc}]^{-3}$ . We have  $\bar{n}P_{\text{gal}}(k, z = 0.9) > 1$  for  $k < 0.2 \text{ hMpc}^{-1}$ , where the shotnoise is subdominant.